

1

2

3       The influence of pilot-scale pyro-gasification

4               and activation conditions on porosity

5               development in activated biochars

6

7

8       Flavia Lega Braghiroli<sup>1</sup>, Hassine Bouafif<sup>2</sup>, Nesrine Hamza<sup>1</sup>,

9       Besma Bouslimi<sup>1</sup>, Carmen Mihaela Neculita<sup>3</sup>, Ahmed Koubaa<sup>1</sup>

10

11

12   <sup>1</sup> Institut de recherche sur les forêts (IRF – Research Forest Institute), Université de Québec en

13   Abitibi-Témiscamingue (UQAT), 445 Boul. de l'Université, Rouyn-Noranda, Québec, QC J9X

14   5E4, Canada

15   <sup>2</sup> Centre Technologique des Résidus Industriels (CTRI, Technology Center for Industrial Waste),

16   Cégep de l'Abitibi-Témiscamingue (Abitibi-Témiscamingue College), 425 Boul. du Collège

17   Rouyn-Noranda, QC J9X 5E5, Canada

18   <sup>3</sup> Research Institute on Mines and Environment (RIME), Université de Québec en Abitibi-

19   Témiscamingue (UQAT), 445 Boul. de l'Université, Rouyn-Noranda, QC J9X 5E4, Canada

20

21

## 22 **Abstract**

23 Few studies have examined the influence of pyro-gasification and activation conditions on porosity  
24 development in activated biochars. In this context, this study investigates the effects of pyro-  
25 gasification temperature (315, 399, and 454 °C), activation temperature (700, 800, and 900 °C),  
26 and activating agent (CO<sub>2</sub> flow rate: 2, 3, and 5 L min<sup>-1</sup>) on porosity in materials made from wood  
27 residues (black spruce and white birch). Activated biochars were prepared in a two-step process:  
28 torrefaction/fast pyrolysis in a pilot-scale plant and activation using an in-house pilot-scale furnace.

29 Results show that the physical properties of activated biochars improved over biochars and wood  
30 residues, with fivefold greater surface area for activated birch biochar over biochars, and threefold  
31 greater surface area for activated spruce biochars. Statistical analysis results reveal that pyro-  
32 gasification and activation temperature, CO<sub>2</sub> gas flow rate, and wood residue type significantly  
33 affected the porosity of activated biochars (at  $p < 0.05$ ). The main findings are as follows: i)  
34 Torrefaction or pyrolysis pre-treatment step had less impact on the porosity of activated biochars,  
35 so lower energy expenditure is required to improve product quality, i.e., porosity; ii) Activation  
36 temperature was the major variable to optimize specific surface area; by increasing from 700 to 900  
37 °C, the average surface area for activated biochars made from both wood residues increased to  
38 nearly 120 m<sup>2</sup> g<sup>-1</sup>; iii) pilot-scale technologies produced porous activated biochars comparable to  
39 laboratory-scale technologies which could boost incentives to use thermochemical biomass  
40 conversion, and increase the profitability with these diversified by-products in biorefinery industry.

41  
42  
43 **Keywords:** Biochar, activated biochar, pyro-gasification and activation conditions, operating  
44 parameters optimization, statistical analysis

## 45 **1. Introduction**

46 Advanced biomass conversion methods (using renewable carbon sources) enable transforming  
47 low-cost waste by-products into value-added materials such as chemicals, plastics, food additives,  
48 clothing fibers, polymers, paint, heat, fuel, and electricity [1–3]. Biomass conversion is a promising  
49 research field that examines and develops sustainable, environmentally friendly products and  
50 practices. The main challenge is to produce cost-efficient materials that perform as well or better  
51 than fossil fuel-based materials [4]. Thermochemical conversion processes (e.g., torrefaction,  
52 pyrolysis, gasification) are used to convert lignocellulosic biomass into solid, liquid, and gas  
53 products at various proportions and with physicochemical properties that are significantly enhanced  
54 over those of the raw material. The solid material produced is called biochar [5], defined by the  
55 International Biochar Initiative (IBI) as a solid material obtained from the thermochemical  
56 conversion of biomass in an oxygen-limited environment [6].

57 Recently, primary industries (e.g., agriculture, logging, forestry) have been converting biomass  
58 residues into biochar to manage the tons of waste generated daily. Biochar can then be  
59 commercialized as fertilizers for soil amendment [7–9] and as pellets for bioenergy production [10].  
60 Recent applications reported in the literature, including carbon sequestration (climate change  
61 mitigation) and degraded site rehabilitation [11–13], have promoted advances in biochar structure  
62 and characteristics, with consequent positive impacts on agriculture and the environment [14].  
63 Moreover, due to the higher carbon content of biochar compared to biomass and the presence of  
64 certain oxygenated groups (e.g., carboxylic, phenolic, carbonyl), biochar has been used as carbon  
65 electrode materials for application in electrochemical capacitors and supercapacitors [15–17],  
66 catalyst supports [18,19], and adsorbents [20]. However, these applications are limited by the  
67 relatively low surface area ( $< 200 \text{ m}^2 \text{ g}^{-1}$ ) and porosity of biochars due to certain limited conditions

68 during large-scale reactor preparation: low-temperature pyro-gasification (e.g., torrefaction at 320  
69 °C max), short residence time (1–2 s), and high heating rate (1000 °C min<sup>-1</sup>).

70 Activation is a commonly used method to improve the **physical** properties and adsorptive  
71 capacity of biochars [21]. Activation refers to chemical and/or physical treatment of biochar that  
72 maximizes the pore density as well as the surface area available for adsorption or chemical  
73 reactions. Typically, biochars are impregnated with chemicals such as H<sub>3</sub>PO<sub>4</sub> or KOH and/or steam  
74 or CO<sub>2</sub> gas at high temperature (e.g., 900 °C), causing a selective gasification of carbon atoms [22].  
75 During this process, low molecular weight carbon molecules are removed, generating voids in the  
76 material structure. Thus, when processed at higher temperature, activated biochar presents **a better**  
77 **developed porous carbon structure** [21]. Several biomass precursors derived from wood residues,  
78 chips and pellets, or agricultural wastes such as fruit shells, stones, husks, and hulls have been used  
79 to produce activated biochars [23]. **Abundant literature** have examined the influence of activation  
80 parameters (e.g., activation temperature, activation time, gas flow rate, impregnation chemical,  
81 biochar ratio) on porosity development in activated biochars [24]. The results show that processing  
82 conditions at high activation temperature (e.g., 900 °C) [25–31], high CO<sub>2</sub> or steam flow rate  
83 [32,33], longer residence time (e.g., 2h) [25,26,32,34–37], and high chemical impregnation ratio  
84 [38–40] produce highly porous materials. However, little attention has been paid to the different  
85 pyro-gasification **(i.e., an integrative term that comprises all thermochemical processes such as**  
86 **torrefaction, slow to fast pyrolysis, and gasification)** conditions for biochar production or how these  
87 conditions affect the porosity of activated biochars.

88 Biochar as a by-product of biomass conversion by pyro-gasification has also been applied as a  
89 precursor for activated biochar production. Azargohar and Dalai [41] investigated biochar  
90 activation using biochar made from wood residues produced by large-scale renewable bio-oil

91 production, whereas Zhang et al. [42] used a pilot fluidized sand-bed reactor ( $7 \text{ kg h}^{-1}$  feed rate) for  
92 fast pyrolysis of biomass wastes (oak wood, corn hulls, and corn stover) at  $500 \text{ }^{\circ}\text{C}$ . For the  
93 activation procedure, the same authors used a small fixed bed reactor to produce chemically  
94 activated carbon (up to  $1578 \text{ m}^2 \text{ g}^{-1}$  surface area) and a small quartz reactor to produce  $\text{CO}_2$ -  
95 activated biochar (up to  $1010 \text{ m}^2 \text{ g}^{-1}$  surface area), respectively. Both activated biochars were  
96 prepared in laboratory-scale furnaces using small amounts of precursor: 20 and 0.7 g, respectively.  
97 In this case, the activation parameters were more controllable due to the small amounts of stationary  
98 precursor. Other authors have prepared activated biochars using a laboratory-scale furnace for both  
99 steps: pyro-gasification and activation [43–50]. Although a pilot-scale activation furnace that would  
100 be readily applicable for industrial-scale production of activated biochar shows great promise, few  
101 studies have investigated the processing conditions for these technologies to date.

102 Moreover, in response to ever stricter government regulations for pollution control, activated  
103 biochars offer an alternative material for the activated carbon market, which is projected to post  
104 \$4.9 billion in revenues by 2021 [51]. For this purpose, activated biochars were prepared using  
105 pilot-scale torrefaction/pyrolysis and activation of different wood residues. The processing  
106 conditions (i.e., parameters) were optimized and statistically analyzed to assess the effects on the  
107 porosity (surface area and pore volume) of the produced materials. Using a statistical model  
108 analysis, the porosity of activated biochars was controlled by varying the processing conditions to  
109 achieve distinct porous materials for specific potential applications. An additional practical  
110 implication of this study is the reduced energy and time required to produce high-quality activated  
111 biochars from wood residues.

## 112 **2. Materials and methods**

### 113 2.1 Biochar preparation

114 Biochars were prepared from black spruce (BS) and white birch (WB) wood residues sampled  
115 from sawmills located in Abitibi-Témiscamingue, in the province of Québec, Canada. This biomass  
116 waste was selected due to its large availability in the region and its successful application as  
117 precursors for biochar production using CarbonFX technology (Airex Energy Inc., Bécancour, QC,  
118 Canada). Fig. 1 a) shows the torrefaction/fast pyrolysis plant where biomass is converted to  
119 torrefied material or biochar (at 250 to 455 °C) in an oxygen-free environment. Materials were  
120 processed in a cyclonic bed reactor enabling large-scale biochar production (250 kg h<sup>-1</sup>) from a  
121 variety of feedstock, including woody biomass and agricultural waste. The biomass is first dried in  
122 a pre-drying system (100-160 ±10 °F), then transported into a conditioning chamber (900-1200 ±20  
123 °F) connected to a combustion chamber (1200 ±20 °F), that heats the whole system. Subsequently,  
124 the biomass reaches the cyclonic bed reactor (600-900 ±20 °F) where it is converted into torrefied  
125 biomass or biochar in approximately 2 s. A panel control controls the whole system notably the  
126 following parameters: temperature process, percentage of oxygen entrance, hot air flow, and  
127 residence time in the cyclonic bed reactor. Wood residues were milled with a 6 mm Hammer Mill  
128 equipped with a screen grate (industrial grinder, Schutte Buffalo, Hammer Mills, Buffalo, NY,  
129 USA) and subsequently dried (dryer, Abri-Tech Inc., Namur, QC, Canada) to obtain a moisture  
130 content below 40% before introduction into the reactor. For each biomass waste (BS or WB), three  
131 types of biochars were synthesized by CarbonFX at three different temperatures: 315, 399, and 454  
132 °C (600, 750, and 850 °F), respectively. The synthesized materials were designated BS315, BS399,  
133 and BS454, and WB315, WB399 and WB454, respectively.

## 134 2.2 Activated biochar synthesis

135 For the activation procedure, each biochar type was placed in an in-house pilot-scale furnace.  
136 Fig. 1 b) shows the 1 kg charge pilot furnace developed at the CTRI laboratory for biochar

137 activation. It comprises three parts: 1) a feed hopper, 2) a screw conveyor tube placed in a muffle  
138 furnace, and 3) a recovery hopper. A condensation tube allows gases and organic compounds  
139 released during activation to be condensed, and additional gas inlets allow introducing nitrogen to  
140 maintain an inert system as well as CO<sub>2</sub> gas as the physical agent. The screw conveyor is driven by  
141 an electronic engine to transport the precursor material (milled at 1–2 mm; grinder: Ro-tap RS-29,  
142 WS Tyler, Mentor, OH, USA) from the feed hopper to the recovery hopper. Activation time was  
143 measured with a chronometer: the material took 67 min to pass through the screw conveyor to the  
144 recovery hopper. 100 g of each biochar type was processed at three different pyrolysis temperatures  
145 (315, 399, and 454 °C), activation temperatures (700, 800, and 900 ± 4 °C), and activation gas  
146 injection rates (2, 3, and 5 L min<sup>-1</sup>). The highest CO<sub>2</sub> flow rate (5 L min<sup>-1</sup>) was applied exclusively  
147 for biochar activation at 900 °C. The biochar materials BS315 and WB454, which were activated  
148 at 900 °C in the presence of CO<sub>2</sub> gas at 5 L min<sup>-1</sup>, were designated BS315A900-5 and WB454A900-  
149 5, respectively.

### 150 2.3 Materials characterization

151 Before and after processing, all the materials were characterized in terms of morphology,  
152 CHNSO percentage, thermal degradation as a function of temperature, porous structure (surface  
153 area and pore volume), and surface chemistry. The morphology of wood residues, biochars, and  
154 activated biochars was investigated with a JEOL JSM-5500 (JEOL USA, Inc., Peabody, MA, USA)  
155 scanning electron microscope (SEM) after metallization (i.e., samples were mounted on gold studs).  
156 CHNS elemental analyzer (Perkin Elmer 2400 CHNS/O Analyzer; Waltham, MA, USA) was used  
157 for elemental determination of carbon, hydrogen, nitrogen, and sulfur contents by sample  
158 combustion in a pure O<sub>2</sub> stream. Oxygen content was obtained by calculating the difference (%O =  
159 100 - %CHNS). Thermogravimetric analysis (TGA) using a Netzsch STA 449 F5 Jupiter

160 instrument (Exton, PA, USA) was performed to determine thermal degradation of woody residues,  
161 biochars, and activated biochars. A 15 mg sample of each material was placed in a ceramic crucible  
162 and the temperature was then increased to 1000 °C at a rate of 10 °C/min<sup>-1</sup>. Analyses were  
163 performed using He gas as a carrier at a flow rate of 50 mL min<sup>-1</sup>. X-ray photoelectron spectroscopy  
164 (XPS) spectra were recorded with a Kratos AXIS ULTRA system (Wharfside, MA, UK) equipped  
165 with a channel electron multiplier detector. The X-ray source used monochromatic Al K-alpha  
166 radiation operated at 300 W under vacuum at 5 x 10<sup>-10</sup> Torr. Binding energies for the high-resolution  
167 spectra were calibrated using C1s at 284.6 eV as a reference. The XPS core level spectra were  
168 analyzed using CasaXPS (Casa Software Ltd.).

169 Pore texture parameters were obtained by Kr and N<sub>2</sub> at -196 °C and by CO<sub>2</sub> at 0 °C using a  
170 Micromeritics ASAP 2460 Surface Area Analyzer (Norcross, GA, USA). N<sub>2</sub> was used to analyze  
171 highly porous materials (i.e., activated biochars), CO<sub>2</sub> to measure ultramicropores (< 0.7 nm)  
172 present in biochars and activated biochars, and Kr to analyze low porous materials (i.e., BS and  
173 WB). Wood residues and biochars were degassed under vacuum for 48 h at 80 and 100 °C,  
174 respectively. Samples after activation at 700, 800 and 900 °C were degassed under vacuum for 48  
175 h at 250 °C prior to adsorption testing. N<sub>2</sub> adsorption isotherms were treated to obtain: (i) the surface  
176 area ( $S_{\text{BET}}$ , m<sup>2</sup> g<sup>-1</sup>) calculated by the Brunauer-Emmet-Teller (BET) model applied to the nitrogen  
177 adsorption data in the appropriate relative pressure range ( $P/P_0$ ) from 0.01 to 0.05 such that the BET  
178 constant ( $C$ ) that provides information about the interaction of the adsorbent surface and the  
179 adsorbate was always positive [52]; (ii) the micropore volume ( $V_{\mu}$ , cm<sup>3</sup> g<sup>-1</sup>) determined by the  
180 Dubinin–Radushkevich (DR) equation [53]; (iii) the total pore volume ( $V_{0.97}$ , cm<sup>3</sup> g<sup>-1</sup>) calculated  
181 from the amount of nitrogen adsorbed at 0.97 relative pressure [54]; and (iv) the mesopore volume  
182 ( $V_m$ , cm<sup>3</sup> g<sup>-1</sup>) calculated as the difference ( $V_{0.97} - V_{\mu}$ ). The pore size distribution (PSD) was  
183 determined by applying density functional theory (DFT) using N<sub>2</sub> adsorption isotherms [55]. The



184 average mesopore diameter ( $d_m$ ) was determined by applying Barret–Joyner–Halenda (BJH)  
185 analysis to the N<sub>2</sub> desorption branch [56].

#### 186 2.4. Statistical analysis

187 The porosity of activated biochars [surface area ( $S_{BET}$ ), total pore volume ( $V_{0.97}$ ), micropore  
188 volume measured by N<sub>2</sub> and CO<sub>2</sub> gases ( $V_{\mu, N_2}$  and  $V_{\mu, CO_2}$ ), and mesopore content (%)] was subjected  
189 to variance analysis with GLM using Type III procedures (partial sums of squares) [57]. GLM  
190 estimates the relative magnitude of each independent variation source: wood residue type (BS,  
191 WB), pyro-gasification temperature (315, 399, and 454 °C), activation temperature (700, 800, and  
192 900 °C) and CO<sub>2</sub> gas flow rate (2 and 3 L min<sup>-1</sup>). Analyses were performed using the following  
193 general linear model (Eq. 1). Only significant interactions were considered in the model, as shown  
194 in Eq. 1.

$$195 \quad Y_{ijkl} = \mu + \alpha_i + \beta_j + \gamma_k + \delta_l + (\alpha\beta)_{ij} + (\alpha\gamma)_{ik} + \varepsilon \quad (1)$$

196 where  $Y_{ijkl}$  is the dependent variable [ $S_{BET}$ ,  $V_{0.97}$ ,  $V_{\mu, N_2}$ ,  $V_{\mu, CO_2}$  and mesopores (%)],  $\mu$  is the overall  
197 mean,  $\alpha_i$  is the wood residue effect,  $\beta_j$  is the pyro-gasification temperature effect,  $\gamma_k$  is the activation  
198 temperature effect,  $\delta_l$  is the CO<sub>2</sub> flow gas effect,  $(\alpha\beta)_{ij}$  is the interaction between wood residue type  
199 and pyro-gasification temperature,  $(\alpha\gamma)_{ik}$  is the interaction between species and activation  
200 temperature, and  $\varepsilon$  is the error term.

201 Data were analyzed with the PROC GLM procedure in SAS<sup>®</sup>, version 9.4 [58]. Statistical  
202 significance was determined using  $F$ -tests at  $p \leq 0.05$ . The assumptions of the analysis of variance  
203 (homoscedasticity and residual normality) were verified. The estimated mean and standard  
204 deviation for each activated biochar property was calculated for each wood residue, pyro-  
205 gasification temperature, activation temperature, and CO<sub>2</sub> gas flow rate. Tukey's studentized range  
206 (honest significant difference – HSD) was used to test significant statistical differences in activated

207 biochar variables between wood residues (BS and WB), pyro-gasification temperatures (315, 399,  
208 and 454 °C), activation temperatures (700, 800 and 900 °C) and CO<sub>2</sub> gas flow rates (2 and 3 L min<sup>-1</sup>).  
209 <sup>1</sup>). *F*-values were considered statistically significant at  $p \leq 0.05$ .

### 210 3. Results and discussion

#### 211 3.1 Morphological, chemical, and thermal analysis

212 The SEM microscopic structure of BS (softwood, broadleaf, deciduous trees, or gymnosperms)  
213 and WB (hardwood, needle-leaved evergreen trees, angiosperms, or flowering plants) from the  
214 temperate part of the Northern Hemisphere is shown in Fig. 2. The SEM images show substantial  
215 differences in cellular structure between the two woods [59]. BS wood is relatively homogeneous,  
216 with a simple structure consisting primarily of overlapping tracheids (fibers) connected by bordered  
217 pits and rays. The WB wood structure is more complex: it is a diffuse-porous wood containing a  
218 relatively high proportion of fibers, vessel elements, and thin-walled ray cells. The rays are mostly  
219 homocellular and 1–3 cells wide. In addition, there are numerous extremely small and diffuse ray-  
220 vessel pits. The structural changes in biochars treated at 315, 399, and 454 °C are illustrated in Fig.  
221 1S (Supplementary Material), showing the presence of grooves and channels. Increasing the pyro-  
222 gasification temperature from 315 to 454 °C enhances the release of low molecular weight volatiles  
223 from the matrix structure, resulting in chars with more rudimentary pores. The pores are irregular  
224 in shape and disposed in a multi-layered structure. However, no significant differences in porous  
225 structure are observed when the pyro-gasification temperature was increased from 315 to 454 °C  
226 (Fig. 1S). Fig. 2S illustrates the structure of activated biochars made from BS and WB treated at  
227 454 °C and activated at 700, 800, and 900 °C with CO<sub>2</sub> at 3 L min<sup>-1</sup> flow rate. The SEM images for  
228 activated biochar showed the development of narrow and larger pores structures, but no clear  
229 structural differences are seen across materials activated at different temperatures.

230 Weight loss (%) for the biomass, biochars (processed at 454 °C), and activated biochars  
231 (processed at 900 °C) was investigated as a function of the temperature range 30–900 °C (Fig 3 a)  
232 and b)). BS and WB showed high thermal degradation in the 100 to 500 °C range: cellulose,  
233 hemicellulose, and lignin in the wood residues were pyrolyzed via different mechanisms and  
234 reaction paths. Decomposition takes place at temperatures ranging from 240 to 350 °C for cellulose  
235 [60,61], 200 to 260 °C for hemicellulose, and 280 to 500 °C for lignin [62–64]. TGA showed that  
236 activated biochars were more thermally stable than unactivated biochars. Only 5.2% and 8.4%  
237 weight were released during thermal degradation of activated biochars prepared at 900 °C for WB  
238 and BS, respectively. This property is important for determining the ability of a given activated  
239 biochar to undergo and endure the thermal regeneration cycles when applied for contaminant  
240 sorption in water and gases [65].

241 The percentages of C, O, and H from several species of wood residues do not present significant  
242 differences but the percentages of cellulose, hemicellulose, lignin and extractives vary significantly.  
243 For example, the carbon content for BS and WB is 48 and 47 %, respectively, whereas the  
244 percentage of lignin in BS (25–28 %) [66] is significantly higher than in WB (17–21 %) [67]. Fast  
245 pyrolysis (at 454 °C) produced a substantial reduction in oxygen and hydrogen content and a  
246 substantial increase in carbon content compared to torrefaction (at 315 °C). The H/C and O/C ratios  
247 were used to predict the variation in biochar aromatization and polarity as a function of pyro-  
248 gasification temperature, respectively. Lower O/C ratio may result in fewer hydrophilic biochars,  
249 whereas lower H/C ratio indicates that the material presents a greater number of aromatic structures,  
250 especially for activated biochars prepared at high temperature (i.e., 900 °C). This finding suggests  
251 that torrefied wood or biochar are still far from being pure carbon so their physical or chemical

252 modification (i.e., activation) is recommended to improve their adsorptive characteristics and  
253 applications.

254 XPS analysis provided information on the carbon bonding states for all materials: wood  
255 residues, biochars, and activated biochars made from BS and WB. The XPS C1s peaks were  
256 deconvoluted and used to estimate the relative proportions of the functional groups listed in Table  
257 1S. The main peak lower than 285 eV for all materials was assigned to aliphatic/aromatic carbon  
258 (C–C, C–H, and C=C). The peaks at 285.7–287.1, 286.1–288, and 288–289.4 eV were then  
259 attached to the oxygen-containing moieties, i.e., C–O, C=O or O–C–O, and O–C=O, respectively  
260 [68]. The spectra for the biochar materials show two predominant peaks of functional groups:  
261 graphitic sp<sup>2</sup> carbon and the C–O bond, found in the range of 61.5–72.0% and 17.1–27.7%,  
262 respectively. The same predominant graphitic sp<sup>2</sup> carbon peaks seen in the biochars increased to  
263 68.3–79.9% for the activated biochars, whereas C–O group peaks reduced to 7.1–12.8% for the  
264 activated biochars. The relative percentages of oxygenated functional groups decreased drastically  
265 at higher pyro-gasification temperature (from 315 to 454 °C) and with subsequent activation (from  
266 700 to 900 °C). Other oxygenated groups accounted for less than 5% content for all materials,  
267 except for WB315 (i.e., 7.2% for C=O and O–C–O groups).

## 268 3.2 Material physical properties

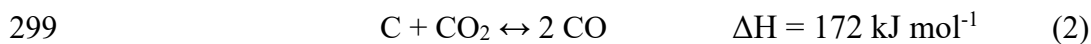
### 269 3.2.1. Characteristics of wood residues, biochars, and activated biochars

270 Birch and spruce wood residues showed very low porosity, up to 0.5 m<sup>2</sup> g<sup>-1</sup>. After  
271 torrefaction/fast pyrolysis of both residues at 315, 399, and 454 °C for 2 s, materials were highly  
272 microporous, presenting ultramicropores (measured by CO<sub>2</sub> adsorption analysis). The final  
273 torrefied wood or biochars presented increases in surface area of 78, 136, and 177 m<sup>2</sup> g<sup>-1</sup> for birch  
274 residues and 42, 158, and 208 m<sup>2</sup> g<sup>-1</sup> for spruce residues at 315, 399, and 454 °C, respectively. The

275 porosity of the biochars also increased at higher pyro-gasification temperature, as confirmed by  
276 studies that used different precursors such as debarked loblolly pine chips [69], date pits [35], or  
277 broiler litter [70]. Activated birch biochar presented a more developed porosity than activated  
278 spruce biochar, with surface area and pore volume ranging from 451  $\text{m}^2 \text{g}^{-1}$  (WB399A700-2) to 881  
279  $\text{m}^2 \text{g}^{-1}$  (WB454A900-3), total pore volume of 0.20 and 0.53  $\text{cm}^3 \text{g}^{-1}$ , respectively, and micropore  
280 volume ranging from 0.18 to 0.33  $\text{cm}^3 \text{g}^{-1}$ . For activated spruce biochar, surface area ranged from  
281 415  $\text{m}^2 \text{g}^{-1}$  (BS399A900-3) to 896  $\text{m}^2 \text{g}^{-1}$  (BS399A900-5), with total pore volume of 0.17 and 0.50  
282  $\text{cm}^3 \text{g}^{-1}$ , respectively, and micropore volume ranging from 0.17 and 0.34  $\text{cm}^3 \text{g}^{-1}$  (Fig. 4).

283 Biochar activation involves a reaction (Boudouard reaction, Eq. 2) between the carbon present  
284 in the biochar materials and injected  $\text{CO}_2$  (C- $\text{CO}_2$  reaction). At high temperatures, this endothermic  
285 reaction promotes the removal of carbon atoms present in the material, increasing the burn-off. The  
286 equilibrium constant of the Boudouard reaction (Eq. 2) does not favor CO production until  
287 temperatures exceed 700 °C [71]. In addition, the increased  $\text{CO}_2$  concentration enhances the C- $\text{CO}_2$   
288 reaction, resulting in increased pore development. It is noteworthy that, for the majority of biochars  
289 and at 900 °C, the porosity was reduced at the higher gas flow rate (5  $\text{L min}^{-1}$ ). For example,  
290 RB454CO2900-2 presented a surface area of 630  $\text{m}^2 \text{g}^{-1}$ , which increased to 873  $\text{m}^2 \text{g}^{-1}$  for  
291 RB454CO2900-3 but decreased to 559  $\text{m}^2 \text{g}^{-1}$  at the highest flow rate (RB454CO2900-5) (Fig. 3S  
292 a)). Similar findings were observed for other biochar types exposed to very high flow rates [44].  
293 The reaction between carbon and  $\text{CO}_2$  resulted not only in the opening of blocked pores to form  
294 new micropores, but also in the widening of existing micropores by a gasification reaction, causing  
295 the formation of mesopores [72]. However, the contact time between the carbon surface and  $\text{CO}_2$   
296 (introduced at high velocity) may have been shortened due to the reduced diffusion into the porous

297 structure. In addition, at longer residence times and higher CO<sub>2</sub> flow rate, micro- and mesopores  
298 formed during activation at high temperature (i.e., 900 °C) may be destroyed to form macropores.



300 The nitrogen adsorption/desorption isotherms at -196 °C for biochars WB454 and BS454  
301 activated at 700, 800, and 900 °C are shown in Fig. 4S a) and b). All the adsorption isotherms  
302 present a similar shape. Nitrogen isotherms are a combination of Type I and Type IV isotherms,  
303 and are characteristic of micro-mesoporous solids according to IUPAC classification [73].  
304 However, activated biochars show the most prominent hysteresis effect at 900 °C, due to the higher  
305 proportion of mesopores compared to at 700 °C. According to their N<sub>2</sub> adsorption isotherms, the  
306 hysteresis loop is Type H4, which features parallel and almost horizontal branches, and is  
307 attributable to the adsorption/desorption in narrow slit-like pores [73]. The accessibility of the  
308 adsorbate molecules to the pores of the adsorbent can be affected by their shape. Therefore, the  
309 access of adsorbate molecules to the slit pores is controlled by the pore width, and is mainly  
310 restricted by the thickness of adsorbate molecules [74]. The pore size distribution shown in Fig. 4S  
311 c) and d) also confirms the presence of mesopores greater than 10 nm in diameter for activated  
312 biochars at 800 and 900 °C, whereas much lower percentages of mesopores were found for  
313 activated biochars at 700 °C. The average pore diameter data for activated birch and spruce biochars  
314 support these results. The smallest pore diameter (up to 3.7 nm) was obtained at 700 °C, whereas  
315 at 900 °C, the average pore diameter increased to up to 6.8 nm, favoring the development of  
316 mesoporosity (Fig. 3S b)).

317 The CO<sub>2</sub> adsorption isotherms at 0 °C for activated biochars made from birch and spruce are  
318 shown in Fig. 4S e) and f), respectively. At this temperature, CO<sub>2</sub> molecules can more easily access  
319 ultramicropores (< 0.7 nm) than N<sub>2</sub> at -196 °C. Activated birch biochars presented higher volume

320 of ultramicropores (up to  $0.28 \text{ cm}^3 \text{ g}^{-1}$ ), as indicated by the  $\text{CO}_2$  adsorption curve compared to  
321 activated spruce biochars (up to  $0.2 \text{ cm}^3 \text{ g}^{-1}$ ). It is noteworthy that WB454A900-3 shows high  
322 versatility: the pore size distribution comprises ultramicropores ( $V_{\text{CO}_2} = 0.28 \text{ cm}^3 \text{ g}^{-1}$ ) as well as  
323  $0.33 \text{ cm}^3 \text{ g}^{-1}$  and  $0.20 \text{ cm}^3 \text{ g}^{-1}$  of micro- and mesopores, respectively. The activated biochars present  
324 a variable range of pores:  $< 0.7 \text{ nm}$ , from 0 to 2 nm, and mesopores (2–10 nm and  $> 10 \text{ nm}$ ),  
325 showing promise for a range of applications in various adsorption fields, including  
326 electrochemistry, catalysis, and contaminant sorption in water.

### 327 3.2.2 Influence of pyro-gasification and activation conditions on the porosity of activated 328 biochars and practical implications

329 Means and variations in the properties of activated biochar made from both wood residues (BS  
330 and WB) are shown in Fig. 4. The analysis of variance (Table 1) shows that, for all variation sources  
331 (pyro-gasification and activation temperature,  $\text{CO}_2$  gas flow rate, and wood residue type), most  
332 biochar porosity features were significantly affected (at  $p < 0.05$ ). Varying the activation  
333 temperature (from 700 to 900 °C) and the  $\text{CO}_2$  flow rate (from 2 to 3  $\text{L min}^{-1}$ ) enhanced the surface  
334 area, pore volume, and mesopore content for both BS and WB wood residues. The average surface  
335 area was 541, 557, and 660  $\text{m}^2 \text{ g}^{-1}$  at 700, 800, and 900 °C for birch, and 490, 537, and 607  $\text{m}^2 \text{ g}^{-1}$   
336 for spruce, respectively (Fig. 4). Multiple comparison tests showed significant differences between  
337 700 and 900 °C and between 800 and 900 °C, as indicated by different superscript letters displayed  
338 in Fig. 4. However, the differences between 700 and 800 °C were not statistically significant (except  
339 for mesopore content). This indicates that activated biochar porosity tends to increase at very high  
340 activation temperature, especially up to 900 °C. In addition, the difference between the two  $\text{CO}_2$   
341 flow rates (2 and 3  $\text{L min}^{-1}$ ) was significant for all porosity properties (Table 1): all porosity  
342 properties increased with increasing  $\text{CO}_2$  flow rate (Fig. 4).

343 In the case of pyro-gasification temperature, the two wood residues showed different trends.  
344 Still, most of the porosity parameters (except for mesopore content) were significantly affected by  
345 increased temperature (at  $p < 0.05$ ) (Table 1). For activated spruce biochars, the temperature  
346 increase from 315 to 454 °C enhanced the average surface area (539 to 584 m<sup>2</sup> g<sup>-1</sup>), pore volume  
347 (0.26 to 0.30 cm<sup>3</sup> g<sup>-1</sup>), and mesopore content (18 to 24%), as seen in Fig. 4. For activated birch  
348 biochars, most of the porosity parameters (except for mesopore content) decreased with temperature  
349 increase from 315 to 454 °C: surface area decreased from 623 to 603 m<sup>2</sup> g<sup>-1</sup> and pore volume from  
350 0.31 to 0.30 cm<sup>3</sup> g<sup>-1</sup>.

351 Based on these findings, we may conclude that the variation due to the activation temperature  
352 exceeded the variation due to the pyro-gasification temperature and the CO<sub>2</sub> flow rate, as indicated  
353 by the higher F-values (Table 1). For instance, for activated spruce biochar, the surface area  
354 increased more (23.9%) with higher activation temperature (from 700 to 900 °C) compared to the  
355 increase (8.3%) with higher pyro-gasification temperature (from 315 to 454 °C) and compared to  
356 the increase (8.5%) with higher flow rate (from 2 to 3 L min<sup>-1</sup>) (Fig. 4). For activated birch biochar,  
357 surface area increased by 22.0 and 9.8% with higher activation temperature (from 700 to 900 °C)  
358 and flow rate (from 2 to 3 L min<sup>-1</sup>), respectively, and decreased by 3.4% with higher pyrolysis  
359 temperature (from 315 to 454 °C).

360 In addition, the interaction between wood residues and activation temperature was significant  
361 for most physical properties of the activated biochars, except for mesopore content (Table 1),  
362 indicating that the effect of activation temperature depends on the type of wood residue. The surface  
363 area of activated biochars made from WB and BS increases linearly with the activation temperature  
364 as shown in Fig. 5S. The variations in surface area (119 m<sup>2</sup> g<sup>-1</sup>) and pore volume (0.11 cm<sup>3</sup> g<sup>-1</sup>) for  
365 WB were almost the same as for BS (117 m<sup>2</sup> g<sup>-1</sup> and 0.08 cm<sup>3</sup> g<sup>-1</sup>, respectively) (Fig. 4). In contrast,



366 the interaction between both wood residue types and pyro-gasification temperature was not  
367 significant for activated biochar porosity, except for mesopore content ( $p = 0.0044$ , [Table 1](#)), where  
368 increased pyro-gasification temperature (from 315 to 454 °C) had a greater effect on WB (6.4%  
369 increase) than on BS (1.4% increase).

370 Few studies have examined the effects of optimized pyro-gasification and activation conditions  
371 on the porosity of activated biochar in terms of the quality of the biomass precursor (i.e., ligno- or  
372 non-lignocellulosic) and the processing conditions (i.e., chemical or physical activation). Oh and  
373 Park [75] reported a substantial increase in surface area up to 330 m<sup>2</sup> g<sup>-1</sup> for KOH-activated rice  
374 husk biochars pyrolyzed at 700 °C ( $S_{\text{BET}} = 2410 \text{ m}^2 \text{ g}^{-1}$ ) compared to 1000 °C ( $S_{\text{BET}} = 2080 \text{ m}^2 \text{ g}^{-1}$ ),  
375 whereas Lua et al. [45] reported a decrease of 176 m<sup>2</sup> g<sup>-1</sup> for CO<sub>2</sub>-activated pistachio nutshell  
376 biochars processed at 500 °C and with posterior activation at 900 °C compared to pre-carbonization  
377 at 1000 °C. Using broiler litter feedstock, the same surface area of 335 m<sup>2</sup> g<sup>-1</sup> was measured for two  
378 biochars processed at pyrolysis temperatures of 350 and 700 °C and posterior activation in the  
379 presence of steam at 800 °C [70].

380 Other authors have found that activation temperature was the most influential variable for  
381 changes in surface area. Azargohar and Dalai [76] used a central composite optimization design to  
382 investigate the impact of steam ratio (0.4–2), activation temperature (600–900 °C), and time (0.9–4  
383 h) on the surface area of activated spruce biochar. Activation temperature was one of the most  
384 influential parameters for increased surface area of activated biochars. Recently, Işıtan *et al.* [29]  
385 used regression analysis to study the impact of pyrolysis and activation temperature on the surface  
386 area of activated pistachio nutshell biochar (prepared in a small-scale furnace) and found that  
387 increasing the temperature from 800 to 900 °C (in the presence of CO<sub>2</sub>) produced a surface area  
388 increase of more than 300 m<sup>2</sup> g<sup>-1</sup> with pre-carbonization temperatures of 450, 550, or 650 °C. The

389 regression analysis indicated that pyrolysis temperature had no significant impact on the surface  
390 area or pore volume of the activated biochars. These findings are in line with the findings of the  
391 present study on the effects of optimized pyro-gasification and activation conditions (using  
392 materials that were prepared in pilot-scale furnaces) on the porosity of activated birch and spruce  
393 biochars. Compared to activation temperature, torrefaction and pyrolysis temperature had lower  
394 impacts on the porosity of CO<sub>2</sub>-activated biochars made from BS and WB residues.

395 Upscaling the production of activated biochars may reduce the efficiency of heating and mass  
396 transfer in the char bed, lowering the porosity of materials compared to other wood waste activated  
397 biochars available in the literature ( $S_{\text{BET}}$  higher than 1000 m<sup>2</sup> g<sup>-1</sup>) [27,42,46]. These high surface  
398 areas were reached through laboratory furnaces where the conditions of temperature and flow gases  
399 were well controlled while N<sub>2</sub> and CO<sub>2</sub> were efficiently in contact with the low amount of material  
400 placed in the furnace in a static position. We have proved in this work that a pilot-scale continuous  
401 system could be an effective alternative to produce porous activated biochars having surface areas  
402 in a range of 400 and 900 m<sup>2</sup> g<sup>-1</sup>. These materials reached surface area values and pore size  
403 distribution comparable with other agricultural waste derived-materials (i.e., pecan shells [77]; rice  
404 straw [78]; palm seed coat [79]; pistachio nut shells [45]; oil-palm shells [80]; nut waste [31]; palm  
405 kernel shells [81,82]; canola meal [83]; corn stalks [84]) prepared in small-scale laboratory  
406 furnaces. In addition, WB and BS activated biochars showed recently to be effective for the removal  
407 of phenolic compounds in synthetic and real effluents [65].

#### 408 4. Conclusion

409 The influence of pyro-gasification temperature and activation conditions on the porosity of  
410 activated biochars made from two wood residues (black spruce and white birch) was investigated  
411 using pilot-scale furnaces for torrefaction/fast pyrolysis and activation. Pyro-gasification and

412 activation temperature, CO<sub>2</sub> gas flow rate, and wood residue type significantly (at  $p < 0.05$ ) affected  
413 most biochar porosity properties (surface area, total pore volume, micropore volume, and mesopore  
414 content). However, activation temperature accounted for more variation than pyro-gasification  
415 temperature or CO<sub>2</sub> gas flow rate. This means that by improving the process efficiency required for  
416 product quality, less heat or energy (at low temperatures) is expended, with no impact on the  
417 porosity of the resultant activated biochars. Further studies are needed to determine whether the  
418 statistical analysis holds true for other types of biomass residue. Comparing to small-scale  
419 laboratory furnaces, upscaling the activation furnace may reduce the efficiency of heating and mass  
420 transfer in the char bed, lowering the porosity of materials. However, porous activated biochars  
421 obtained in a range of 400 and 900 m<sup>2</sup> g<sup>-1</sup> were comparable with agricultural waste activated  
422 biochars available in the literature and produced through laboratory-scale furnaces. Therefore, the  
423 pilot-scale technologies used in this study to produce activated biochars from wood residues could  
424 boost economic incentives to apply thermochemical biomass conversion processes and to develop  
425 new and diversified products (not only biochar, bio-oil, or syngas, but also activated biochar) that  
426 would be highly profitable for the biorefinery industry.

427

428

429

430

431

432

433

434  
435  
436  
437  
438  
439  
440  
441  
442  
443  
444  
445  
446  
447  
448  
449  
450  
451  
452  
453  
454

**Acknowledgments**

This study was supported by Québec’s Ministry of Economy, Science and Innovation (Ministère de l’Économie, de la Science et de l’Innovation du Québec), the Natural Sciences and Engineering Research Council of Canada (NSERC), the Canada Research Chair Program, Abitibi-Témiscamingue College, and the Technology Center for Industrial Waste (Centre Technologique des Résidus Industriels) through its partner on this project, Airex Energy. The first author, Dr. Flavia Lega Braghiroli, sincerely acknowledges financial support by the NSERC via a Banting Postdoctoral Fellowship (2017–2019). The authors also thank Mr. Gilles Villeneuve for the assistance with both furnaces, analysis and testing in the laboratory.

455

456

457

458

459

460

461

462

463

464 **References**

- 465 [1] R. Mülhaupt, Green polymer chemistry and bio-based plastics: dreams and reality,  
466 *Macromol. Chem. Phys.* 214 (2013) 159–174. doi:10.1002/macp.201200439.
- 467 [2] S. Tojo, T. Hirasawa, *Research Approaches to Sustainable Biomass Systems*, 1st ed.,  
468 Academic Press, Waltham, MA, 2013.
- 469 [3] S.K. Brar, S.J. Sarma, K. Pakshirajan, *Platform chemical biorefinery: future green*  
470 *chemistry*, 1st ed., Elsevier Inc, Waltham, MA, 2016.
- 471 [4] Ed de Jong, Adrian Higson, Patrick Walsh, Maria Wellisch, *Bio-based chemicals. Value*  
472 *added products from biorefineries*, IEA Bioenergy - Task 42 Biorefineries, 2012.
- 473 [5] P. Basu, *Biomass Gasification, Pyrolysis and Torrefaction: Practical Design and Theory*,  
474 2nd ed., Academic Press, San Diego, CA, 2013.
- 475 [6] IBI, International Biochar Initiative, (2012). <http://www.biochar-international.org/> (accessed  
476 January 21, 2018).
- 477 [7] W. Wu, M. Yang, Q. Feng, K. McGroutner, H. Wang, H. Lu, Y. Chen, Chemical  
478 characterization of rice straw-derived biochar for soil amendment, *Biomass Bioenergy*. 47  
479 (2012) 268–276. doi:10.1016/j.biombioe.2012.09.034.
- 480 [8] A. Ahmed, J. Kurian, V. Raghavan, Biochar influences on agricultural soils, crop  
481 production, and the environment: a review, *Environ. Rev.* 24 (2016) 495–502.  
482 doi:10.1139/er-2016-0008.
- 483 [9] M. Ahmad, S.S. Lee, S.E. Lee, M.I. Al-Wabel, D.C.W. Tsang, Y.S. Ok, Biochar-induced  
484 changes in soil properties affected immobilization/mobilization of metals/metalloids in  
485 contaminated soils, *J. Soils Sediments*. 17 (2017) 717–730. doi:10.1007/s11368-015-1339-4.
- 486 [10] Q. Hu, J. Shao, H. Yang, D. Yao, X. Wang, H. Chen, Effects of binders on the properties of  
487 bio-char pellets, *Appl. Energy*. 157 (2015) 508–516. doi:10.1016/j.apenergy.2015.05.019.

- 488 [11] J. Lehmann, J. Gaunt, M. Rondon, Bio-char sequestration in terrestrial ecosystems – a  
489 review, *Mitig. Adapt. Strateg. Glob. Change.* 11 (2006) 395–419. doi:10.1007/s11027-005-  
490 9006-5.
- 491 [12] L. Beesley, E. Moreno-Jiménez, J.L. Gomez-Eyles, E. Harris, B. Robinson, T. Sizmur, A  
492 review of biochars’ potential role in the remediation, revegetation and restoration of  
493 contaminated soils, *Environ. Pollut.* 159 (2011) 3269–3282.  
494 doi:10.1016/j.envpol.2011.07.023.
- 495 [13] J. Lehmann, S. Joseph, eds., *Biochar for Environmental Management: Science, Technology  
496 and Implementation*, Routledge, Abingdon, UK, 2015.
- 497 [14] F.-C. Wu, R.-L. Tseng, Preparation of highly porous carbon from fir wood by KOH etching  
498 and CO<sub>2</sub> gasification for adsorption of dyes and phenols from water, *J. Colloid Interface Sci.*  
499 294 (2006) 21–30. doi:10.1016/j.jcis.2005.06.084.
- 500 [15] J. Jiang, L. Zhang, X. Wang, N. Holm, K. Rajagopalan, F. Chen, S. Ma, Highly ordered  
501 macroporous woody biochar with ultra-high carbon content as supercapacitor electrodes,  
502 *Electrochimica Acta.* 113 (2013) 481–489. doi:10.1016/j.electacta.2013.09.121.
- 503 [16] L. Zhang, J. Jiang, N. Holm, F. Chen, Mini-chunk biochar supercapacitors, *J. Appl.  
504 Electrochem.* 44 (2014) 1145–1151. doi:10.1007/s10800-014-0726-7.
- 505 [17] A.M. Dehkhoda, E. Gyenge, N. Ellis, A novel method to tailor the porous structure of KOH-  
506 activated biochar and its application in capacitive deionization and energy storage, *Biomass  
507 Bioenergy.* 87 (2016) 107–121. doi:10.1016/j.biombioe.2016.02.023.
- 508 [18] J.R. Kastner, J. Miller, D.P. Geller, J. Locklin, L.H. Keith, T. Johnson, Catalytic  
509 esterification of fatty acids using solid acid catalysts generated from biochar and activated  
510 carbon, *Altern. Sources Catal. Mater.* 190 (2012) 122–132.  
511 doi:10.1016/j.cattod.2012.02.006.
- 512 [19] R. Ormsby, J.R. Kastner, J. Miller, Hemicellulose hydrolysis using solid acid catalysts  
513 generated from biochar, *Altern. Sources Catal. Mater.* 190 (2012) 89–97.  
514 doi:10.1016/j.cattod.2012.02.050.
- 515 [20] M. Ahmad, A.U. Rajapaksha, J.E. Lim, M. Zhang, N. Bolan, D. Mohan, M. Vithanage, S.S.  
516 Lee, Y.S. Ok, Biochar as a sorbent for contaminant management in soil and water: a review,  
517 *Chemosphere.* 99 (2014) 19–33. doi:10.1016/j.chemosphere.2013.10.071.
- 518 [21] H. Marsh, F. Rodríguez-Reinoso, *Activated carbon*, 1st ed., Elsevier, Amsterdam, NL, 2006.
- 519 [22] F. Rodríguez-Reinoso, M. Molina-Sabio, Activated carbons from lignocellulosic materials  
520 by chemical and/or physical activation: an overview, *Carbon.* 30 (1992) 1111–1118.  
521 doi:10.1016/0008-6223(92)90143-K.
- 522 [23] X. Tan, S. Liu, Y. Liu, Y. Gu, G. Zeng, X. Hu, X. Wang, S. Liu, L. Jiang, Biochar as  
523 potential sustainable precursors for activated carbon production: multiple applications in  
524 environmental protection and energy storage, *Bioresour. Technol.* 227 (2017) 359–372.  
525 doi:10.1016/j.biortech.2016.12.083.
- 526 [24] P. González-García, Activated carbon from lignocellulosics precursors: a review of the  
527 synthesis methods, characterization techniques and applications, *Renew. Sustain. Energy  
528 Rev.* 82 (2018) 1393–1414. doi:10.1016/j.rser.2017.04.117.
- 529 [25] A. Baçaoui, A. Yaacoubi, A. Dahbi, C. Bennouna, R. Phan Tan Luu, F.J. Maldonado-Hodar,  
530 J. Rivera-Utrilla, C. Moreno-Castilla, Optimization of conditions for the preparation of  
531 activated carbons from olive-waste cakes, *Carbon.* 39 (2001) 425–432. doi:10.1016/S0008-  
532 6223(00)00135-4.

- 533 [26] Y.-J. Zhang, Z.-J. Xing, Z.-K. Duan, Meng Li, Y. Wang, Effects of steam activation on the  
534 pore structure and surface chemistry of activated carbon derived from bamboo waste, *Appl.*  
535 *Surf. Sci.* 315 (2014) 279–286. doi:10.1016/j.apsusc.2014.07.126.
- 536 [27] C. Grima-Olmedo, Á. Ramírez-Gómez, D. Gómez-Limón, C. Clemente-Jul, Activated  
537 carbon from flash pyrolysis of eucalyptus residue, *Heliyon.* 2 (2016) 1–18.  
538 doi:10.1016/j.heliyon.2016.e00155.
- 539 [28] J. Guo, A.C. Lua, Characterization of adsorbent prepared from oil-palm shell by CO<sub>2</sub>  
540 activation for removal of gaseous pollutants, *Mater. Lett.* 55 (2002) 334–339.  
541 doi:10.1016/S0167-577X(02)00388-9.
- 542 [29] S. Işıtan, S. Ceylan, Y. Topcu, C. Hintz, J. Tefft, T. Chellappa, J. Guo, J.L. Goldfarb,  
543 Product quality optimization in an integrated biorefinery: conversion of pistachio nutshell  
544 biomass to biofuels and activated biochars via pyrolysis, *Energy Convers. Manag.* 127  
545 (2016) 576–588. doi:10.1016/j.enconman.2016.09.031.
- 546 [30] S.-H. Jung, J.-S. Kim, Production of biochars by intermediate pyrolysis and activated  
547 carbons from oak by three activation methods using CO<sub>2</sub>, *J. Anal. Appl. Pyrolysis.* 107  
548 (2014) 116–122. doi:10.1016/j.jaap.2014.02.011.
- 549 [31] V. Sricharoenchaikul, C. Pechyen, D. Aht-ong, D. Atong, Preparation and characterization  
550 of activated carbon from the pyrolysis of physic nut (*Jatropha curcas* L.) waste, *Energy*  
551 *Fuels.* 22 (2008) 31–37. doi:10.1021/ef700285u.
- 552 [32] D. Chen, X. Chen, J. Sun, Z. Zheng, K. Fu, Pyrolysis polygeneration of pine nut shell:  
553 quality of pyrolysis products and study on the preparation of activated carbon from biochar,  
554 *Bioresour. Technol.* 216 (2016) 629–636. doi:10.1016/j.biortech.2016.05.107.
- 555 [33] I.M. Lima, D.L. Boykin, K. Thomas Klasson, M. Uchimiya, Influence of post-treatment  
556 strategies on the properties of activated chars from broiler manure, *Chemosphere.* 95 (2014)  
557 96–104. doi:10.1016/j.chemosphere.2013.08.027.
- 558 [34] M. Fan, W. Marshall, D. Dugaard, R.C. Brown, Steam activation of chars produced from  
559 oat hulls and corn stover, *Bioresour. Technol.* 93 (2004) 103–107.  
560 doi:10.1016/j.biortech.2003.08.016.
- 561 [35] C. Bouchelta, M.S. Medjram, M. Zoubida, F.A. Chekkat, N. Ramdane, J.-P. Bellat, Effects  
562 of pyrolysis conditions on the porous structure development of date pits activated carbon, *J.*  
563 *Anal. Appl. Pyrolysis.* 94 (2012) 215–222. doi:10.1016/j.jaap.2011.12.014.
- 564 [36] B. del Campo, Production of activated carbon from fast pyrolysis biochar and the  
565 detoxification of pyrolytic sugars for ethanol fermentation, Graduate Theses and  
566 Dissertations, paper 14691, Iowa State University, 2015. <http://lib.dr.iastate.edu/etd/14691>.
- 567 [37] G. Selvaraju, N.K.A. Bakar, Production of a new industrially viable green-activated carbon  
568 from *Artocarpus integer* fruit processing waste and evaluation of its chemical,  
569 morphological and adsorption properties, *J. Clean. Prod.* 141 (2017) 989–999.  
570 doi:10.1016/j.jclepro.2016.09.056.
- 571 [38] D. Angın, T.E. Köse, U. Selengil, Production and characterization of activated carbon  
572 prepared from safflower seed cake biochar and its ability to absorb reactive dyestuff, *Appl.*  
573 *Surf. Sci.* 280 (2013) 705–710. doi:10.1016/j.apsusc.2013.05.046.
- 574 [39] H. Mao, D. Zhou, Z. Hashisho, S. Wang, H. Chen, H.H. Wang, Preparation of pinewood-  
575 and wheat straw-based activated carbon via a microwave-assisted potassium hydroxide  
576 treatment and an analysis of the effects of the microwave activation conditions,  
577 *BioResources.* 10 (2014) 809–821. doi:10.15376/biores.10.1.809-821.

- 578 [40] J. Zhang, J. Liu, R. Liu, Effects of pyrolysis temperature and heating time on biochar  
579 obtained from the pyrolysis of straw and lignosulfonate, *Bioresour. Technol.* 176 (2015)  
580 288–291. doi:10.1016/j.biortech.2014.11.011.
- 581 [41] R. Azargohar, A.K. Dalai, Biochar as a precursor of activated carbon, *Appl. Biochem.*  
582 *Biotechnol.* 131 (2006) 762–773. doi:10.1385/ABAB:131:1:762.
- 583 [42] T. Zhang, W.P. Walawender, L.T. Fan, M. Fan, D. Daugaard, R.C. Brown, Preparation of  
584 activated carbon from forest and agricultural residues through CO<sub>2</sub> activation, *Chem. Eng. J.*  
585 105 (2004) 53–59. doi:10.1016/j.cej.2004.06.011.
- 586 [43] A. Baçaoui, A. Yaacoubi, A. Dahbi, C. Bennouna, J. Ayele, M. Mazet, Activated carbon  
587 production from Moroccan olive wastes - influence of some factors, *Environ. Technol.* 19  
588 (1998) 1203–1212. doi:10.1080/09593331908616780.
- 589 [44] T. Yang, A.C. Lua, Characteristics of activated carbons prepared from pistachio-nut shells  
590 by physical activation, *J. Colloid Interface Sci.* 267 (2003) 408–417. doi:10.1016/S0021-  
591 9797(03)00689-1.
- 592 [45] A.C. Lua, T. Yang, J. Guo, Effects of pyrolysis conditions on the properties of activated  
593 carbons prepared from pistachio-nut shells, *J. Anal. Appl. Pyrolysis.* 72 (2004) 279–287.  
594 doi:10.1016/j.jaap.2004.08.001.
- 595 [46] Y. Ngernyen, C. Tangsathitkulchai, M. Tangsathitkulchai, Porous properties of activated  
596 carbon produced from eucalyptus and wattle wood by carbon dioxide activation, *Korean J.*  
597 *Chem. Eng.* 23 (2006) 1046–1054. doi:10.1007/s11814-006-0028-9.
- 598 [47] A. Veksha, P. Pandya, J.M. Hill, The removal of methyl orange from aqueous solution by  
599 biochar and activated carbon under microwave irradiation and in the presence of hydrogen  
600 peroxide, *J. Environ. Chem. Eng.* 3 (2015) 1452–1458. doi:10.1016/j.jece.2015.05.003.
- 601 [48] D. Feng, Y. Zhao, Y. Zhang, S. Sun, S. Meng, Y. Guo, Y. Huang, Effects of K and Ca on  
602 reforming of model tar compounds with pyrolysis biochars under H<sub>2</sub>O or CO<sub>2</sub>, *Chem. Eng.*  
603 *J.* 306 (2016) 422–432. doi:10.1016/j.cej.2016.07.065.
- 604 [49] U. Iriarte-Velasco, I. Sierra, L. Zudaire, J.L. Ayastuy, Preparation of a porous biochar from  
605 the acid activation of pork bones, *Food Bioprod. Process.* 98 (2016) 341–353.  
606 doi:10.1016/j.fbp.2016.03.003.
- 607 [50] C.M. Park, J. Han, K.H. Chu, Y.A.J. Al-Hamadani, N. Her, J. Heo, Y. Yoon, Influence of  
608 solution pH, ionic strength, and humic acid on cadmium adsorption onto activated biochar:  
609 experiment and modeling, *J. Ind. Eng. Chem.* 48 (2017) 186–193.  
610 doi:10.1016/j.jiec.2016.12.038.
- 611 [51] TechSci Research, Global activated carbon market by type (powdered activated carbon,  
612 granular activated carbon and others), by raw material (wood, coconut shells, coal and  
613 others), by application, competition forecast and opportunities, 2011-2021, (2016).  
614 [https://www.techsciresearch.com/news/1203-activated-carbon-market-size-set-to-cross-4-9-](https://www.techsciresearch.com/news/1203-activated-carbon-market-size-set-to-cross-4-9-billion-by-2021.html)  
615 [billion-by-2021.html](https://www.techsciresearch.com/news/1203-activated-carbon-market-size-set-to-cross-4-9-billion-by-2021.html) (accessed July 1, 2017).
- 616 [52] S. Brunauer, P.H. Emmett, E. Teller, Adsorption of gases in multimolecular layers, *J. Am.*  
617 *Chem. Soc.* 60 (1938) 309–319. doi:10.1021/ja01269a023.
- 618 [53] M.M. Dubinin, Fundamentals of the theory of adsorption in micropores of carbon  
619 adsorbents: Characteristics of their adsorption properties and microporous structures,  
620 *Carbon.* 27 (1989) 457–467. doi:10.1016/0008-6223(89)90078-X.
- 621 [54] S.J. Gregg, K.S.W. Sing, Adsorption, surface area, and porosity, Academic Press, London,  
622 1991.
- 623 [55] P. Tarazona, Solid-fluid transition and interfaces with density functional approaches, *Proc.*  
624 *14th Eur. Conf. Surf. Sci.* 331 (1995) 989–994. doi:10.1016/0039-6028(95)00170-0.



- 625 [56] E.P. Barrett, L.G. Joyner, P.P. Halenda, The determination of pore volume and area  
626 distributions in porous substances. I. Computations from nitrogen isotherms, *J. Am. Chem.*  
627 *Soc.* 73 (1951) 373–380. doi:10.1021/ja01145a126.
- 628 [57] SAS/STAT® 9.2, User's Guide, the GLM procedure, SAS Institute Inc., Cary, NC, 2008.
- 629 [58] SAS, SAS Institute Inc., Cary, NC, 2018.
- 630 [59] R.M. Rowell, ed., *Handbook of wood chemistry and wood composites*, 2nd ed., CRC Press,  
631 Boca Raton, 2013.
- 632 [60] A. Pandey, T. Bhaskar, M. Stöcker, R. Sukumaran, eds., *Recent Advances in*  
633 *Thermochemical Conversion of Biomass*, 1st ed., Elsevier, Amsterdam, NL, 2015.
- 634 [61] W.K. Tang, W.K. Neill, Effect of flame retardants on pyrolysis and combustion of  $\alpha$ -  
635 cellulose, *J. Polym. Sci. Part C Polym. Symp.* 6 (2007) 65–81.  
636 doi:10.1002/polc.5070060109.
- 637 [62] B.V. Babu, Biomass pyrolysis: a state-of-the-art review, *Biofuels Bioprod. Biorefining.* 2  
638 (2008) 393–414. doi:10.1002/bbb.92.
- 639 [63] D. Mohan, Pittman Jr. Charles U., P.H. Steele, Pyrolysis of wood/biomass for bio-oil: a  
640 critical review, *Energy Fuels.* 20 (2006) 848–889. doi:10.1021/ef0502397.
- 641 [64] E.J. Soltes, T.J. Elder, Pyrolysis, in: I.S. Goldstein (Ed.), *Org. Chem. Biomass*, CRC Press,  
642 Boca Raton, FL, 1981: pp. 63–95.
- 643 [65] F.L. Braghiroli, H. Bouafif, N. Hamza, C.M. Neculita, A. Koubaa, Production,  
644 characterization, and potential of activated biochar as adsorbent for phenolic compounds  
645 from leachates in a lumber industry site, *Environ. Sci. Pollut. Res.* (2018).  
646 doi:10.1007/s11356-018-2712-9.
- 647 [66] S.Y. Zhang, A. Koubaa, Forintek Canada Corp, *Softwoods of eastern Canada: their silvics,*  
648 *characteristics, manufacturing and end-uses*, Forintek Canada Corp., Québec, 2007.
- 649 [67] A. Koubaa, W. Belhadef, S. Migneault, *Transformation des bois de trituration de feuillus*  
650 *durs : revue de littérature portant sur les produits et les marchés des essences de bouleau*  
651 *blanc*, Université du Québec en Abitibi-Témiscamingue, Rouyn-Noranda, QC, Canada,  
652 2015.
- 653 [68] A. Lazzarini, A. Piovano, R. Pellegrini, G. Leofanti, G. Agostini, S. Rudić, M.R. Chierotti,  
654 R. Gobetto, A. Battiato, G. Spoto, A. Zecchina, C. Lamberti, E. Groppo, A comprehensive  
655 approach to investigate the structural and surface properties of activated carbons and related  
656 Pd-based catalysts, *Catal. Sci. Technol.* 6 (2016) 4910–4922. doi:10.1039/C6CY00159A.
- 657 [69] J. Park, I. Hung, Z. Gan, O.J. Rojas, K.H. Lim, S. Park, Activated carbon from biochar:  
658 influence of its physicochemical properties on the sorption characteristics of phenanthrene,  
659 *Bioresour. Technol.* 149 (2013) 383–389. doi:10.1016/j.biortech.2013.09.085.
- 660 [70] M. Uchimiya, L.H. Wartelle, I.M. Lima, K.T. Klasson, Sorption of deisopropylatrazine on  
661 broiler litter biochars, *J. Agric. Food Chem.* 58 (2010) 12350–12356.  
662 doi:10.1021/jf102152q.
- 663 [71] J. Hunt, A. Ferrari, A. Lita, M. Crosswhite, B. Ashley, A.E. Stiegman, Microwave-specific  
664 enhancement of the carbon–carbon dioxide (Boudouard) reaction, *J. Phys. Chem. C.* 117  
665 (2013) 26871–26880. doi:10.1021/jp4076965.
- 666 [72] H. Marsh, ed., *Activated Carbon Compendium: A Collection of Papers from the Journal*  
667 *Carbon 1996-2000*, Gulf Professional Publishing, North Shields, UK, 2001.
- 668 [73] K.S.W. Sing, Reporting physisorption data for gas/solid systems with special reference to  
669 the determination of surface area and porosity (Recommendations 1984), *Pure Appl. Chem.*  
670 57 (1985) 603–619. doi:10.1351/pac198557040603.

- 671 [74] Y. Guo, S. Kaplan, T. Karanfil, The significance of physical factors on the adsorption of  
672 polyaromatic compounds by activated carbons, *Carbon*. 46 (2008) 1885–1891.  
673 doi:10.1016/j.carbon.2008.07.032.
- 674 [75] G.H. Oh, C.R. Park, Preparation and characteristics of rice-straw-based porous carbons with  
675 high adsorption capacity, *Fuel*. 81 (2002) 327–336. doi:10.1016/S0016-2361(01)00171-5.
- 676 [76] R. Azargohar, A.K. Dalai, Steam and KOH activation of biochar: experimental and  
677 modeling studies, *Microporous Mesoporous Mater.* 110 (2008) 413–421.  
678 doi:10.1016/j.micromeso.2007.06.047.
- 679 [77] M. Ahmedna, W.E. Marshall, R.M. Rao, Production of granular activated carbons from  
680 select agricultural by-products and evaluation of their physical, chemical and adsorption  
681 properties<sup>1</sup>, *Bioresour. Technol.* 71 (2000) 113–123. doi:10.1016/S0960-8524(99)00070-X.
- 682 [78] C.H. Yun, Y.H. Park, C.R. Park, Effects of pre-carbonization on porosity development of  
683 activated carbons from rice straw, *Carbon*. 39 (2001) 559–567. doi:10.1016/S0008-  
684 6223(00)00163-9.
- 685 [79] S. Rengaraj, S.-H. Moon, R. Sivabalan, B. Arabindoo, V. Murugesan, Agricultural solid  
686 waste for the removal of organics: adsorption of phenol from water and wastewater by palm  
687 seed coat activated carbon, *Waste Manag.* 22 (2002) 543–548. doi:10.1016/S0956-  
688 053X(01)00016-2.
- 689 [80] A.C. Lua, F.Y. Lau, J. Guo, Influence of pyrolysis conditions on pore development of oil-  
690 palm-shell activated carbons, *J. Anal. Appl. Pyrolysis*. 76 (2006) 96–102.  
691 doi:10.1016/j.jaap.2005.08.001.
- 692 [81] N.S. Nasri, U.D. Hamza, S.N. Ismail, M.M. Ahmed, R. Mohsin, Assessment of porous  
693 carbons derived from sustainable palm solid waste for carbon dioxide capture, *Spec. Vol.*  
694 *PSE Asia Clean. Prod.* 71 (2014) 148–157. doi:10.1016/j.jclepro.2013.11.053.
- 695 [82] U.D. Hamza, N.S. Nasri, N.S. Amin, J. Mohammed, H.M. Zain, Characteristics of oil palm  
696 shell biochar and activated carbon prepared at different carbonization times, *Desalination*  
697 *Water Treat.* 57 (2016) 7999–8006. doi:10.1080/19443994.2015.1042068.
- 698 [83] N. Rambabu, B.V.S.K. Rao, V.R. Surisetty, U. Das, A.K. Dalai, Production,  
699 characterization, and evaluation of activated carbons from de-oiled canola meal for  
700 environmental applications, *Ind. Crops Prod.* 65 (2015) 572–581.  
701 doi:10.1016/j.indcrop.2014.09.046.
- 702 [84] Z. Wang, J. Wu, T. He, J. Wu, Corn stalks char from fast pyrolysis as precursor material for  
703 preparation of activated carbon in fluidized bed reactor, *Bioresour. Technol.* 167 (2014)  
704 551–554. doi:10.1016/j.biortech.2014.05.123.
- 705  
706  
707  
708  
709  
710  
711  
712  
713  
714  
715  
716  
717

718  
719  
720  
721  
722  
723  
724  
725  
726  
727  
728  
729  
730  
731  
732  
733  
734  
735  
736  
737  
738  
739

**Table captions:**

740  
741

**Table 1:** Analysis of variance (GLM) with *F*-values and their significance for each source of variation in the physical properties of activated biochars

742 **Figure captions:**

743  
744  
745

**Fig. 1:** a) Pilot-scale fast pyrolysis unit (CarbonFX, Airex Energy); b) Biochar activation furnace developed at CTRI (Centre Technologique des Résidus Industriels – Technology Center for Industrial Waste), QC, Canada.

746  
747

**Fig. 2:** SEM images of the two wood residues used in the present study: a) white birch (WB); and b) black spruce (BS).

748  
749

**Fig. 3:** Weight loss as a function of the temperature range 30–900 °C (TG and DTG curves) for: a) WB, WB454, and WB454CO2900-3; and b) BS, BS454, and BS454CO2900-3.

750 **Fig. 4:** Least squares mean for biochar properties (surface area, total pore volume, micropore  
751 volume measured by N<sub>2</sub> and CO<sub>2</sub> gases, and mesopore content) for each activation  
752 temperature (700, 800, and 900 °C) and pyro-gasification temperature (315, 399, and 454  
753 °C), CO<sub>2</sub> flow rate (2 and 3 L min<sup>-1</sup>), and wood residue type (WB and BS); and multiple  
754 comparison tests. Different superscript letters (i.e., a, b, ac) displayed in the graph indicates  
755 significant difference at  $p = 0.05$ . Bars indicate estimated standard errors.

756  
757  
758  
759  
760

761 **Table 1:** Analysis of variance (GLM) with *F*-values and their significance for each source of variation in the **physical** properties of activated biochars

762

Source of variation	Wood residues (WR)		Pyro-gasification temperature (PT)		Activation temperature (AT)		CO <sub>2</sub> Flow rate		WR*PT		WR*AT	
	<i>df</i>	<i>1</i>	<i>2</i>	<i>2</i>	<i>2</i>	<i>1</i>	<i>2</i>	<i>2</i>	<i>2</i>	<i>2</i>		
	<i>F-value</i>	<i>p-value</i>	<i>F-value</i>	<i>p-value</i>	<i>F-value</i>	<i>p-value</i>	<i>F-value</i>	<i>p-value</i>	<i>F-value</i>	<i>p-value</i>	<i>F-value</i>	<i>p-value</i>
S <sub>BET</sub>	12.64	0.0012	5.56	0.0087	13.18	<0.0001	8.44	0.0067	0.63	<b>0.54</b>	4.08	0.0267
V <sub>0.97</sub>	8.48	0.0066	7.27	0.0026	15.98	<0.0001	6.97	0.0129	0.77	<b>0.47</b>	4.27	0.0230
V <sub>μ,N<sub>2</sub></sub>	8.32	0.0071	3.59	0.0395	11.43	0.0002	6.72	0.0144	0.82	<b>0.4483</b>	4.51	0.0191
V <sub>μ,CO<sub>2</sub></sub>	7.07	0.0123	1.37	<b>0.2696</b>	6.64	0.0040	3.06	0.0904	0.90	<b>0.4173</b>	3.86	0.0317
Mesopore (%)	7.36	0.0108	13.47	<0.0001	16.63	<0.0001	1.51	<b>0.2278</b>	6.48	0.0044	0.67	<b>0.5195</b>

**df:** Degrees of freedom; Numbers in bold exceed 0.05 (*p-value*).

763  
764  
765  
766  
767  
768  
769  
770  
771  
772  
773  
774  
775  
776  
777